Experimental and Numerical Study of Low Temperature Methane Steam Reforming for Hydrogen Production

Khzouz, M & Gkanas, E

DOI 10.3390/catal8010005
ISSN 2073-4344
ESSN 2073-4344

Publisher: MDPI

catalysts

MDPI

Article

Experimental and Numerical Study of Low Temperature Methane Steam Reforming for Hydrogen Production

Martin Khzouz * and Evangelos I. Gkanas

Hydrogen and Mobility Lab, Institute for Future Transport and Cities, Coventry University, Cheetah Road, Chamber House IV09, Coventry CV1 2TL, UK; ac1029@coventry.ac.uk

* Correspondence: ac2127@coventry.ac.uk

Received: 15 November 2017; Accepted: 20 December 2017; Published: 25 December 2017

Abstract: Low temperature methane steam reforming for hydrogen production, using experimental developed Ni/Al_2O_3 catalysts is studied both experimentally and numerically. The catalytic activity measurements were performed at a temperature range of 500–700 °C with steam to carbon ratio (S/C) of 2 and 3 under atmospheric pressure conditions. A mathematical analysis to evaluate the reaction feasibility at all different conditions that have been applied by using chemical equilibrium with applications (CEA) software and in addition, a mathematical model focused on the kinetics and the thermodynamics of the reforming reaction is introduced and applied using a commercial finite element analysis software (COMSOL Multiphysics 5.0). The experimental results were employed to validate the extracted simulation data based on the yields of the produced H_2, CO_2 and CO at different temperatures. A maximum hydrogen yield of 2.7 mol/mol-CH_4 is achieved at 700 °C and S/C of 2 and 3. The stability of the $10\%Ni/Al_2O_3$ catalyst shows that the catalyst is prone to deactivation as supported by Thermogravimetric Analysis TGA results.

Keywords: hydrogen production; methane steam reformer; reforming catalysts; reforming modelling; Ni based catalyst

1. Introduction

Methane steam reforming is considered a widely available method to produce hydrogen at large-scale due to the well-developed methane infrastructures and the favorably high hydrogen to carbon ratio of methane [1]. The fuel cell technology requires compact and low cost reformers [2]. The compact reformers should operate at low temperature (<700 °C) and low-pressure conditions (<3 bar). Thus, the current existing large-size reformer technology operating under high temperature (>800 °C) and high-pressure is not suitable for smaller-size reformers for fuel cell applications [3]. Methane steam reforming is a strongly endothermic reaction as shown in Equation (1). It also includes the exothermic water gas shift reaction (Equation (2)) which is more favorable at low temperature conditions (200–550 °C). The total reforming process is described by Equation (3) as a combination of reactions Equations (1) and (2) [4–7].

$$CH_4 + H_2O \rightleftharpoons CO + 3H_2 \qquad \Delta H^\circ_{298} = +206\ kJ/mol \tag{1}$$

$$CO + H_2O \rightleftharpoons CO_2 + H_2 \qquad \Delta H^\circ_{298} = -41\ kJ/mol \tag{2}$$

$$CH_4 + 2H_2O \rightleftharpoons CO_2 + 4H_2 \qquad \Delta H^\circ_{298} = +165\ kJ/mol \tag{3}$$

Nickel-based catalysts are normally used for methane steam reforming. Reforming over supported nickel catalysts has been used commercially for more than 40 years [8]. Such catalysts are designed

to operate at severe reaction temperatures ranging from 700 °C to 1000 °C and high pressure (up to 30 bar) [9]. The Ni-based catalysts are used due to their high conversion activity and low cost [5,10]. It is established that the metal and the support could provide ideal characteristic properties of reforming catalyst [5]. The challenges for nickel catalysts for steam methane reforming are; catalytic activity, Sulphur (S) poisoning, carbon formation and sintering [8]. Therefore, the effects of calcination temperature, nickel loading, reaction temperature and different supports have been investigated in literature [11]. In previous studies, it was mentioned that methane reacts with steam at temperatures over 800 °C when using nickel catalysts [7,12,13]. Ni-based catalysts are very active for reforming reactions and, compared to noble metals are cheaper and easier to handle [5]. Thus, many improvements of their stability regarding sintering and carbon formation were investigated for high temperature operations.

The advantage of performing the steam reforming process at low operating temperatures is the fact that the applied temperature will favors the water gas shift reaction as the CO amount will be suppressed [14]. Consequently, the catalyst must present high performance at low reaction temperatures for conversion of CO via water gas shift reaction. As a consequence, for successful low methane operation temperatures, a reforming catalyst with high activity is required. Another advantage of performing low temperature steam methane reforming is the suitability for chemical looping. The chemical looping of steam methane reforming (CL-SMR), is an alternative chemical process used to produce hydrogen/syngas. It is applied widely on large-scale industrial processes due to the low cost, easy accessibility and environmental-friendly nature [15]. It is normally used to maximize the average methane conversion and hydrogen production yield by employing nickel based oxygen carrier catalysts [16]. The temperature range of such process is between 500 and 750 °C [16]. Sorption enhanced reduction of the nickel oxygen carrier catalyst is used in chemical looping, aiming to capture CO_2 during conventional steam reforming [17]. The nickel oxygen carrier particles should be thermodynamically capable of converting large amounts of methane to synthesis gas [18].

The non-promoted nickel catalysts presented on previous studies is the Ni-rich catalysts which mainly consist of dispersed NiO over Al_2O_3 species [19–21] making the catalyst suitable for high temperature reactions (above 800 °C) where temperature and partial pressure of water vapor during the process are taken into account [22].

Furthermore, when Ni-based catalysts participated in reactions at temperatures above 650 °C the catalysts tend to become deactivated due to the sintering and the carbon formation that will prevent the active metals to perform the catalytic surface reaction [23,24]. The activity of Ni-based catalysts depend on the dispersion of Ni, which is affected on the metal loading and the surface area of the support used [25,26]. It was reported that Ni-based catalysts, can be deactivated easily due to coking and sintering of Ni metal [27], however; this can be solved by optimizing the catalyst contents regarding the Ni loading levels for the selected operation conditions as discussed and studied in the current work. The catalytic methane steam reforming is a surface reaction, thus increasing the amount of active Ni, will increase the surface area, and so the activity the reforming process. Hence, the Ni loading above 15–20 wt % will not increase the catalyst activity, due to poorly dispersion of the additional metal. The catalyst activity decreases per unit metal surface area with increasing the Ni loading above 20 wt % [28–30]. As a result, the active metal surface is limited due to heat and mass transfer effects. Therefore, in the present work, the catalyst prepared has been optimized to 10 wt %, to achieve a high catalytic activity by using the impregnation method.

The main drawback of methane steam reforming reactions at low temperatures, is the development of an active catalyst which can achieve conversion up to equilibrium values [31–33]. Several researchers studied the performance of catalysts in methane steam reforming at temperatures over 700 °C [34–38]. However, the interest on low temperature methane steam reforming catalysts has been recently investigated by considering the importance of using bimetallic catalysts and promoters for the low temperature reaction [32]. The current work includes the performance study of mono-nickel

catalysts at low temperatures supported with catalytic thermodynamics analysis of steam reforming, while at previous studies noble metals (Co., Ru, Rh, Pd, Pt) were added to Ni catalysts in order to enhance the catalytic activation [39–41]. In addition, the Ni catalysts modified with noble metals claimed to be resistive to carbon deposition and catalyst oxidation [39–41]. Liu et al. [42] reviewed the preparation progress of Ni catalysts for steam methane reforming. They indicated the importance of improved Ni catalyst design for coke resistance. Furthermore, they discussed about the importance of using promoters and the effect of the supporting materials. Thus, the importance of catalytic reaction regarding the operating conditions wasn't covered in detail. Nickel catalysts are susceptible to deactivation from the deposition of carbon, even when operating at steam-to-carbon ratios predicted to be thermodynamically outside of the carbon-forming regime which require further research of modifying Ni surfaces with a promoter or preparation techniques [43].

Thermodynamic analysis of equilibrium conditions in the steam reforming of methane, leads to the product enhancement at low cost, considering several operative parameters such as the ratio of steam per methane in the inlet of a reformer, the operating temperature and the pressure [44]. The optimal operating conditions and reactor structures were studied according to the maximum thermochemical energy storage efficiency [45]. The comparison of the simulation results with experimentally obtained data for nickel based catalysts under oxidative reforming conditions was studied for isothermal flow reactor [46].

In the current work, the development of low Ni-loading catalysts, for low temperature methane steam reforming was analyzed and discussed. An extensive experimental study for investigating the activity and stability of such catalysts was performed at different operating conditions, followed by an accurate and detailed thermodynamic equilibrium analysis to study and identify limitations of the reaction and make sure that the proposed reaction is thermodynamically feasible and stable. Finally, a mathematically model was introduced in order to describe the reaction of the hydrogen production and a simulation study by using commercial available finite element analysis software (COMSOL Multiphysics 5.0) was performed for the validation of the reaction performance.

2. Experimental Procedure

2.1. Synthetic Routes

Catalysts with the stoichiometry 10 wt % Ni/Al_2O_3 synthesised via the impregnation method. Commercial nickel nitrate ($Ni(NO_3)_2 \cdot 6H_2O$) (Fisher Scientific, Loughborough, UK) was dissolved in high purity ethanol (99.8%) using a magnetic stirrer and the solution was mixed for 30 min. After the end of this process, 6 g of trilobe Al_2O_3 (Johnson Matthey, Royston, UK) were added to the prepared mixture and mixed for two hours using an ultrasonic bath (Bandelin Sonorex, Berlin, Germany) at 27 °C. The catalyst was dried overnight in a static oven at 100 °C. During the final preparation stage, the catalyst was heated for calcination to 500 °C at a rate of 5 °C/min, held at that temperature for 5 h, then finally cooled at rate 5 °C/min to ambient room temperature.

2.2. Catalyst Characterization

The catalysts were characterized using; Scanning Electron Microscopy (SEM-EDS), nitrogen adsorption-desorption cycles analysed by the Brunauer Emmett Teller (BET) method, Temperature Programmed Reduction (TPR) and ThermoGravimetric Analysis (TGA).

2.2.1. Scanning Electron Microscopy (SEM)

SEM micrographs of the catalyst were performed for both as-synthesized and reacted catalysts (Philips XL-30 SEM, Amsterdam, The Netherlands). The SEM (Energy Dispersive EDS) captures adjusted angle from 15° to 130° upon a 50 × 50 mm stage. The images were recorded and analyzed using INCA software.

2.2.2. Nitrogen Adsorption-Desorption (BET)

In order to determine the catalytic surface area for the as-synthesized and the reacted catalysts, the samples were analyzed by the nitrogen adsorption-desorption method. The measurements were carried out at 1.4 g of catalyst sample using a Micrometrics ASAP 2010 analyzer (Micromeritics, Norcross, GA, USA). Accelerated Surface Area and Porosimetry (ASAP) uses the static volumetric technique to determine surface area using nitrogen physisorption isotherms at −196 °C. The volume of gas adsorbed was recorded by the instrument. Then the experimental data were used to calculate the BET surface area [47].

2.2.3. Temperature-Programmed Reduction (TPR)

The TPR runs were conducted using Micrometrics AutoChem 2920 Analyzer on 1 g of fresh catalyst (as-synthesized). The sample was pretreated with argon gas at flow rate 50 mL/min by increasing the temperature up to 500 °C at a rate of 10 °C/min and held for one hour in order to remove any moisture from the sample and tube; then the sample was cooled down to ambient temperature. After that, 10%H_2/90%Ar at flow rate of 50 mL/min was introduced and the temperature was increased to 900 °C at 10 °C/min to record hydrogen uptake using thermal conductivity detector (TCD). The TPR peak area and the temperatures where the maximum reduction occurs were recorded. The volume of hydrogen uptake was analyzed by converting the area data using pre-defined calibration file where the concentration of the gas was determined.

2.2.4. Thermo Gravimetric Analysis (TGA)

A TGA was carried out using NETZSCH TG 209 F1. The sample was introduced to the chamber in an aluminum crucible that can resist high temperature increase. During the TGA process, the carbon deposited on the catalyst was removed by oxidation using air flow (50 mL/min) and heating of the sample (20 mg) in the oven chamber from 25 °C to 900 °C (10 °C/min). The accumulated carbon in grams for the reaction duration was calculated and the catalyst selectivity for solid carbon (Sel_C) was estimated as shown in Equation (4).

$$Sel_C(\%) = 100 \times \frac{n_{carbon}}{n_{CH_4,in}} \quad (4)$$

where n_i is the total number of moles for species i.

2.3. Catalytic Activity Test

The reaction of methane steam reforming was investigated in terms of reaction conditions, fuel conversion and the amount of H_2, CO_2 and CO produced. The experimental rig consisted of three modules; the feed, the reactor and the gas analysis modules as illustrated in Figure 1a. The feeding module is composed of a Cole-Parmer EW-74930-05 (London, UK) series one pump which can supply water to the vaporization zone and reactor. The heating tape (Omega Engineering FGR-100, Stamford, CT, USA) was wrapped around the feed pipe to generate steam at 110 °C and controlled by using West 2300 PID controller. Digital Brooks mass flow controllers were used to control the flow rate of the various gases fed to the reactor during the catalytic tests. The reactor module consisted of a high temperature furnace (Severn Thermal Solutions Ltd., Dursley, UK) that can withstand temperatures up to 1200 °C and controlled via EUROTHERM PID controller. Inside the furnace, the fixed bed reactor was constructed of stainless steel tube (316L SS) with inner diameter 10.9 mm, wall thickness 0.89 mm and tube length of 395 mm (Figure 1b). The prepared catalyst (3 g) was packed into the reactor and the void space above and below was filled with glass beads; the catalyst bed height was estimated 50 mm in the center of the reactor as shown in Figure 1b. The temperature of the reactor was measured using a K type thermocouple fixed near the center of the bed. The reformate stream at the outlet of the reactor was cooled before proceeding for gas analysis. Therefore, a condenser facilitated by ice

cubes in a bath, surrounding a coiled section of the reactor outlet pipe at a temperature of −2 °C was used. After cooling, the un-reacted liquid was separated from gaseous stream in a specially designed gas-liquid separator unit. The reformate gases were sampled using an online connection to Agilent 7890A model gas analyzer (Santa Clara, CA, USA). The gas sample duration was five minutes before the generated gas withdrawn out to the vent. Prior to the reaction, the system was purged with nitrogen for five minutes to remove the air from the pipes and the reactor bed. Then, hydrogen at flow rate of 10 mL/min was introduced to reduce the catalyst at its reduction temperature (650 °C) determined from TPR test. The reduction process was carried out by raising the temperature to its target point at a rate of 5 °C/min and maintaining it for 30 min in hydrogen flow before switching to pure nitrogen for purging. Methane steam reforming was carried out at temperatures 500, 550, 600, 650 and 700 °C. Pure methane (99.99%) was injected into the reactor feed line at a flow rate of 25 mL/min. The steam generated through the trace heating was mixed with methane at mole ratios of 2:1 and 3:1, with the flow rate being controlled using the pump.

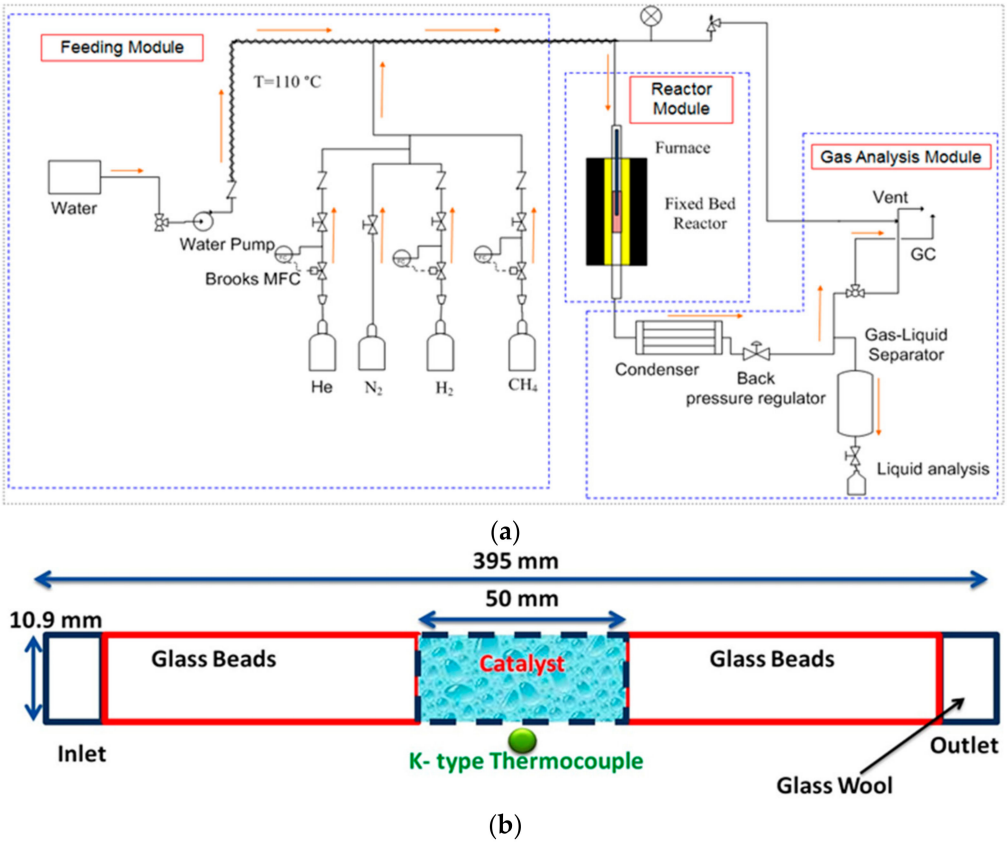

Figure 1. Experimental test rig: (**a**) flow sheet diagram for methane steam reforming activity test and (**b**) fixed bed tube diagram.

3. Numerical Analysis

3.1. Activity Test Calculations

In order to calculate the conversions and the yields of the reaction products, an elemental analysis using the concentrations of CO, CO_2, CH_4 and H_2 at the reactor exit and the inlet flow of methane was performed. The unmeasured amount of water was also calculated. The total molar flow of carbon

entering the reactor from methane equals the carbon leaving the reactor outlet. Equation (5) presents the carbon balance that contains the unknown $\dot{n}_{out,dry}$.

$$\begin{array}{l}\left(y_{CO} + y_{CO_2} + y_{CH_4}\right) \times \dot{n}_{out,dry} = 1 \times \dot{n}_{CH_4,in} \\ y_i = mol\ fraction\ of\ species\ i. \\ \dot{n} = total\ molar\ flow\ rate\ (mol/\min) \\ \dot{n}_i = molar\ flow\ rate\ of\ species\ i\ (mol/\min)\end{array} \quad (5)$$

The hydrogen mass balance analysis was performed as shown in Equation (6), which takes into account the unknown terms, $\dot{n}_{out,dry}$, $\dot{n}_{H_2O,out}$.

$$\begin{array}{l}\left(2y_{H_2} + 4y_{CH_4}\right) \times \dot{n}_{out,dry} + 2 \times \dot{n}_{H_2O,out} = 4 \times \dot{n}_{CH_4,in} + 2 \times \dot{n}_{H_2O,in} \\ y_i = mol\ fraction\ of\ species\ i. \\ \dot{n} = total\ molar\ flow\ rate\ (mol/\min) \\ \dot{n}_i = molar\ flow\ rate\ of\ species\ i\ (mol/\min)\end{array} \quad (6)$$

From the above elemental analysis, the unknown $\dot{n}_{out,dry}$ was measured in the experiment using a bubble flow meter after water condensation and $\dot{n}_{H_2O,out}$ was calculated. The conversions for methane and water were obtained from Equations (7) and (8).

$$\chi_{CH_4} = \frac{\dot{n}_{CH_4,in} - \dot{n}_{CH_4,out}}{\dot{n}_{CH_4,in}} \quad (7)$$

$$\chi_{H_2O} = \frac{\dot{n}_{CH_4,in} - \dot{n}_{CH_4,out}}{\dot{n}_{CH_4,in}} \quad (8)$$

The molar flow rates of the individual products (i) from the reaction were calculated from:

$$\dot{n}_{i,out} = y_i \times \dot{n}_{out,dry} \quad (9)$$

The products yields for H_2, CO_2 and CO were obtained in mol/min per mol/min of methane as shown in Equations (10)–(12).

$$H_2 yield = \frac{\dot{n}_{H_2,out}}{\dot{n}_{CH_4,in}} \quad (10)$$

$$CO_2 yield = \frac{\dot{n}_{CO_2,out}}{\dot{n}_{CH_4,in}} \quad (11)$$

$$CO\ yield = \frac{\dot{n}_{CO,out}}{\dot{n}_{CH_4,in}} \quad (12)$$

3.2. Chemical Equilibrium Analysis

The chemical equilibrium reaction was calculated by using a Chemical Equilibrium Analysis CEA software. The results of the equilibrium analysis are presented in terms of fuel conversion and product yields from the predicted mole fractions of the CEA software. The methane steam reforming was programmed to run with all possible products by entering the moles of methane (1 mol) and water (S/C of 2 and 3). All possible products were considered, but those whose mole fractions were less than 5×10^{-6} were considered as negligible in the calculations. In order to study the conversions and

product yields, the total number of moles in the equilibrium product was calculated by applying the mass balance for carbon (Equation (13)). The Equation (13) contains the unknown term n_{out}.

$$\begin{array}{l}\left(1 \times y_{CO} + 1 \times y_{CO_2} + 1 \times y_{CH_4} + 1 \times y_C\right) \times n_{out} = 1 \times n_{CH_4,in} \\ y_i = mol\ fraction\ of\ species\ i,\ obtained\ from\ CEA\ program \\ n = total\ number\ of\ moles\end{array} \quad (13)$$

3.3. Mathematical Model

3.3.1. Kinetic Parameters

The main chemical reactions involved in the steam methane reforming process have been already described (Equations (1)–(3); several other reactions may occur during the reforming process, but in the current study, the above equations will be taken into account. A number of kinetic [6] expressions describing the methane steam reforming based on empirical models have been described. The reactor used in the current model is based on the experimental rig which is presented in Figure 1b.

The kinetic rates of the adsorption or the production of the gas species, based on the partial pressures, temperatures and species composition are given by the following equations [48].

$$R_1 = \frac{k_1}{p_{H_2} \cdot DEN^2} \cdot \left\{ p_{CH_4} \cdot p_{H_2O} - \frac{{p_{H_2}}^2 \cdot p_{CO}}{K_1} \right\} \quad (14)$$

$$R_2 = \frac{k_2}{p_{H_2O} \cdot DEN^2} \cdot \left\{ p_{CO} \cdot p_{H_2O} - \frac{p_{H_2} \cdot p_{CO_2}}{K_2} \right\} \quad (15)$$

$$R_3 = \frac{k_3}{{p_{H_2}}^{3.5} \cdot DEN^2} \cdot \left\{ p_{CH_4} \cdot {p_{H_2O}}^2 - \frac{{p_{H_2}}^4 \cdot p_{CO_2}}{K_3} \right\} \quad (16)$$

$$DEN = 1 + K_{CH_4} \cdot p_{CH_4} + K_{CO} \cdot p_{CO} + K_{H_2} \cdot p_{H_2} + \frac{K_{H_2O} \cdot p_{H_2O}}{p_{H_2}} \quad (17)$$

The above kinetics is based on the Langmuir-Hinshelwood reaction mechanism. The rate constants and adsorption constants are Arrhenius based function type equations.

$$k_j = A_j \cdot e^{-\frac{E_j}{R_u \cdot T}},\ \mathrm{j} = 1, 2, 3 \quad (18)$$

$$K_J = B_i \cdot e^{-\frac{\Delta_i}{R_u \cdot T}},\ i = CH_4, H_2, H_2O, CO, CO_2 \quad (19)$$

3.3.2. Governing Equations

The mathematical model of a steam reforming reactor is based on theoretical equations that describe the transport phenomena of mass, energy and species chemical reactions.

Energy Equation

The energy conservation equation that has been introduced in the current study is described by the following form.

$$\rho_{mix} \cdot C_p \cdot \vec{u} \cdot \nabla T = \lambda \cdot (\nabla^2 T) + Q \quad (20a)$$

where C_p is the heat capacity of the gas under constant pressure (J/kg/K), ρ is the density of the gas (kg/m^3), u is the velocity (m/s), T is the temperature (K), λ is the thermal conductivity (W/mK) and Q represents the heat source term (W/m^3).

The heat source term is updated by the following:

$$Q = \rho_{mix} \cdot (-\Delta H_1 \cdot k_1 + \Delta H_2 \cdot k_2 - \Delta H_3 \cdot k_3) \quad (20b)$$

where ρ is the mixture density (kg/m^3), ΔH_1 (kJ/kg) is the enthalpy for the first reaction and k_1 (1/s) is the rate constant for the reaction. ΔH_2 (kJ/kg) and ΔH_3 (kJ/kg) is the enthalpy for reaction 2 and 3 respectively. k_2 and k_3 are the reaction rate constants for reaction 2 and 3.

The heat exchange between the reforming area and the external heating jacket is described by;

$$-\hat{n} \cdot (\lambda \cdot \nabla T) = h_t \cdot (\mathrm{T_{ext}} - \mathrm{T}) \tag{21}$$

where h_t is the heat transfer coefficient (W/m^{2}K) and $\mathrm{T_{ext}}$ is the temperature of the heating jacket (K). Due to the highly endothermic nature of the reforming reaction, a large amount of heat has to be supplied to the bed in order to fulfil the thermal energy adsorbed by the reactions. The inward heat flux is described by the right hand term in Equation (21).

Mass Balance

The mass conservation equation applied to the current numerical model is given by the following equation;

$$\frac{\partial}{\partial t} \cdot (\rho \cdot \omega_i) + \nabla(\rho \cdot \omega_i \cdot \vec{u}) = -\nabla j_i + R_i \tag{22}$$

where R_i represents the source term for the rate of production or depletion of the species i (kg/m^{3}s), u is the velocity (m/s), j_i is the mass flux vector (kg/s m) and ω_i is the concentration of species (mol/m^3).

For the steam reforming reaction, the mass terms will be the following:

$$R_{\mathrm{H_2}} = (3 \cdot \mathrm{R_1} + \mathrm{R_2} + 4 \cdot \mathrm{R_3}) \cdot Mm_{\mathrm{H_2}} \tag{23}$$

$$R_{\mathrm{CH_4}} = -(\mathrm{R_1} + \mathrm{R_3}) \cdot Mm_{\mathrm{CH_4}} \tag{24}$$

$$R_{\mathrm{H_2O}} = -(\mathrm{R_1} + \mathrm{R_2} + 2 \cdot \mathrm{R_3}) \cdot Mm_{\mathrm{H_2O}} \tag{25}$$

$$R_{\mathrm{CO}} = (\mathrm{R_1} - \mathrm{R_2}) \cdot Mm_{\mathrm{CO}} \tag{26}$$

3.3.3. Initial and Boundary Conditions

At the beginning of the reaction, the temperature of both the reaction bed and the inlet gases (CH_4 and H_2O) are at the temperature set by the experiment.

$$T_{bed} = T_{\mathrm{CH_4}} = T_{\mathrm{H_2O}} = T_{in} \tag{27}$$

Regarding the species conservation, the composition of the species is given in mass fraction terms. At the beginning of the reaction, the gases within the reactor are CH_4 and H_2O, where the initial conditions have been set for these two species while for the other gases (H_2, CO_2 and CO) the mass fraction is equal to zero.

4. Results and Discussion

4.1. SEM

The SEM (EDS) images of the prepared 10%Ni/Al_2O_3 catalysts are presented in Figure 2. Figure 2a shows an irregular distribution of spherical Ni species (bright white spheres, highlighted by a marked red circle) upon a dark grey substrate of Al_2O_3, indicating large quantities of Al_2O_3 support.

The micrograph of the 10%Ni catalyst after reacted at 500 °C is illustrated in Figure 2b. The presence of holes (highlighted by a marked black circle) over a grey Al_2O_3 support was observed. The SEM image of the 10%Ni catalyst reacted at 700 °C is presented in Figure 2c; white spots which represent Ni species were also observed (highlighted by a marked red circle) distributed over the grey Al_2O_3 support. Agglomeration (highlighted by the green circle) has been observed on the catalyst compared to 10%Ni used catalyst reacted at 500 °C.

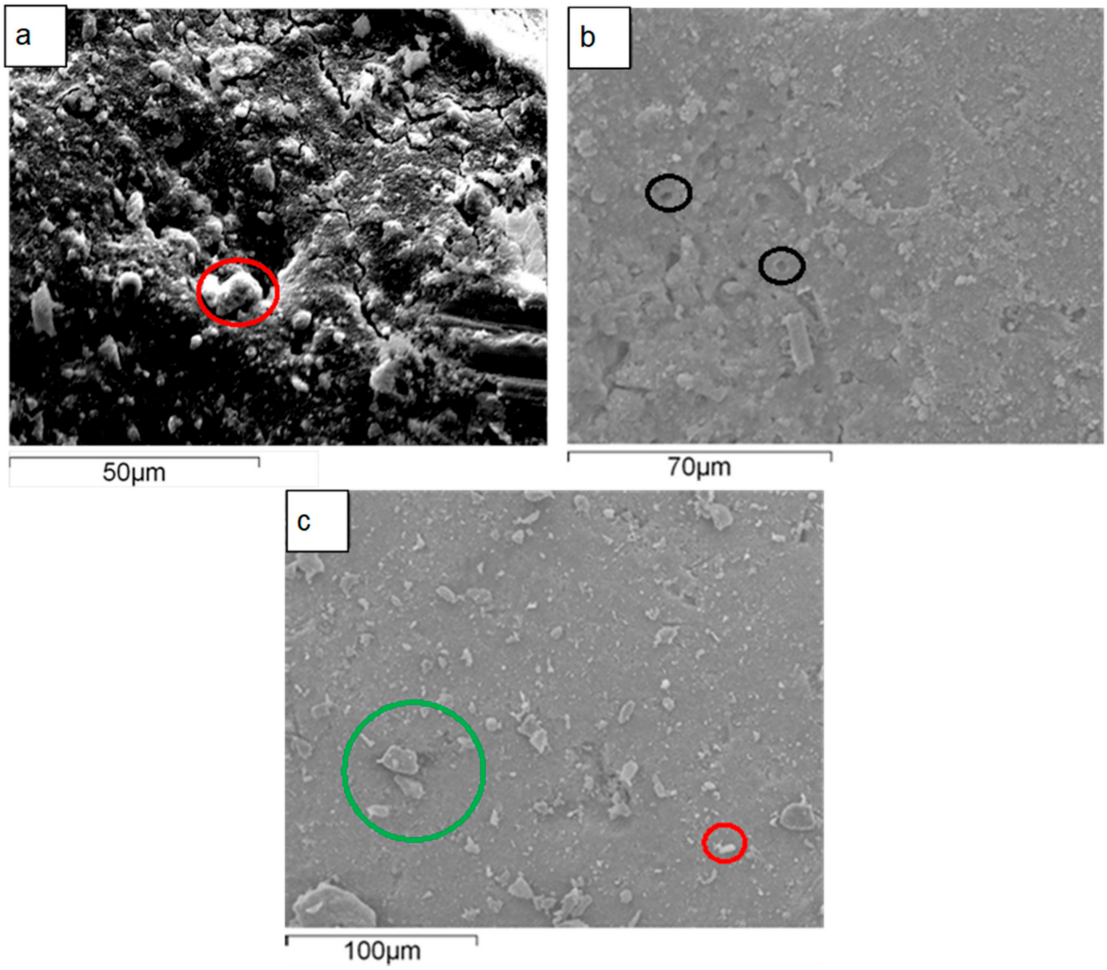

Figure 2. SEM (EDS) micrographs of as-synthesized and reacted catalysts at 500 °C and 700 °C and Steam to Carbon Ratio S/C = 3: (**a**) 10%Ni as-synthesized, (**b**) 10%Ni reacted at 500 °C and (**c**) 10%Ni reacted at 700 °C.

4.2. Nitrogen Adsorption-Desorption

The surface area of trilobe alumina used as support for the impregnated samples was 142 m^2/g. The impregnated samples revealed a lower surface area with respect to the pure alumina. Table 1 presents the BET calculations for the as-prepared catalysts. The used catalysts operated at 700 °C showed lower surface area than the used catalysts operated at 500 °C. This fact justifies the negative effect of high operating temperature on the catalyst surface area.

Table 1. BET surface area for the fresh and used methane catalysts reacted at 500 °C and 700 °C at Steam to Carbon Ratio S/C of 3.

Surface Area (m^2/g)	10%Ni
As-synthesized	122
Reacted at 500 °C	93.3
Reacted at 700 °C	86.1

4.3. TPR

The 10%Ni catalyst displayed broad multi peaks at 400 °C and 650 °C as illustrated in Figure 3. These peaks are attributed to a range of interactions between NiO and the Al_2O_3 support. The low

reduction temperature (400 °C) corresponds to a weak interaction between NiO and Al_2O_3 support and the high reduction temperature (650 °C) is likely to be related to a strong interaction of NiO and Al_2O_3 [49,50].

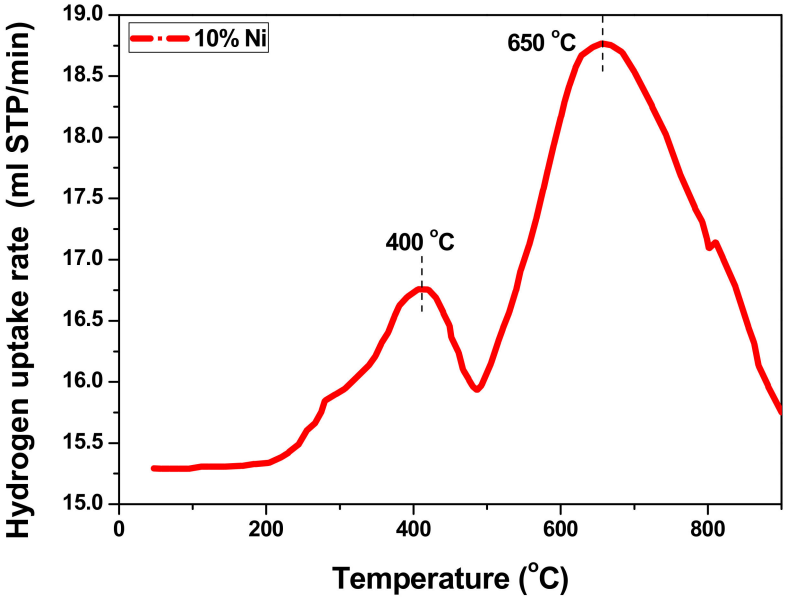

Figure 3. Temperature-Programmed Reduction (TPR) of 10%Ni/Al_2O_3 catalyst.

4.4. Catalytic Reactivity and Equilibrium Analysis Results

The experiments were performed at low methane steam reforming temperature range between 500–700 °C, with the S/C ratio of 2 and 3 under atmospheric pressure. The gas hourly space velocity (GHSV) was 1067.4 h^{-1} for steam reforming at S/C of 2 and 1388.9 h^{-1} at S/C of 3. Both effects from increasing the reaction temperature and increasing the amount of water in the reactants upon the product produced were compared to the calculated equilibrium product yields.

The methane conversion, water conversion and product yields within 500–700 °C and steam to carbon ratios of 2 and 3 are shown in Figure 4. The calculated methane conversion (Figure 4a) increased with increasing the reaction temperature and the amount of water in the reactants (Figure 4b). The calculated H_2 yield increased with increasing temperature and with increasing the amount of water in the reactants (Figure 4c). The calculated CO_2 yield increased and reached a peak at 600 °C then slightly decreased while increasing temperature (Figure 4d). The CO_2 yield increased with increasing the S/C in the reactants (Figure 4d). The calculated CO yield increased with increasing temperature and decreased with the amount of water in the reactants (Figure 4e).

The experimental results showed that the conversion of methane increased with the temperature increase (Figure 4a). The conversion of methane was increased from 32% at 500 °C to 92% at 700 °C for S/C of 3. The results support that the methane reforming reaction is an endothermic process which is enhanced at high temperatures. It was also observed experimentally that with increasing the amount of water in the reactants from S/C of 2 to 3, the methane conversion was not affected much. The amount of water consumed (Figure 4b) was less than the predicted one by the equilibrium analysis (S/C of 3) and is nearly equal for the case of S/C = 2. This behavior can be explained by the longer contact time (residence time) for S/C of 2 (3.37 s) than S/C of 3 (2.59 s).

The amount of hydrogen produced increases at higher temperatures as shown in Figure 4c. The experimental results follow the same trend with the hydrogen yield obtained from equilibrium calculations and are approaching the calculated values at 500–700 °C for S/C = 2. However, the yield of hydrogen produced experimentally for S/C = 3 is less than the calculated results since the amount of water consumed (Figure 4b) was less than the predicted from the numerical equilibrium calculations.

The experimental data showed a maximum hydrogen yield of 2.7 mol/mol-CH_4 at 700 °C and S/C of 2 (Figure 4c), and a minimum hydrogen yield of 1.0 mol/mol-CH_4 at 500 °C and S/C of 3.

Figure 4d presents the amount of CO_2 produced. The CO_2 increases with increasing the temperature, reaching a maximum yield at 600 °C (0.40 mol/mol-CH_4 for S/C = 3 and 0.23 mol/mol-CH_4 for S/C = 2), then it slightly decreases at temperatures 650–700 °C due to the reversible water gas shift reaction. From Figure 4d, the CO_2 content rises (between 500 and 600 °C) with increasing S/C ratio according to the water gas shift reaction equilibrium, since the reaction moves towards the products. The amount of CO_2 decreased at 650–700 °C due to less favorable water gas shift reaction.

Figure 4e shows that the CO produced was monotonically increased with increasing temperature. It was also shown experimentally that by increasing the molar ratio of water in the reactants from 2 to 3, it reveals only a small reduction on the amount of CO produced at 650–700 °C. The amount of CO increased from 0.02 mol/mol-CH_4 to 0.47 mol/mol-CH_4 within the temperature range 500–700 °C for S/C of 3. This explains that CO is produced by increasing the reaction temperature via both methane reaction and reverse water gas shift reaction.

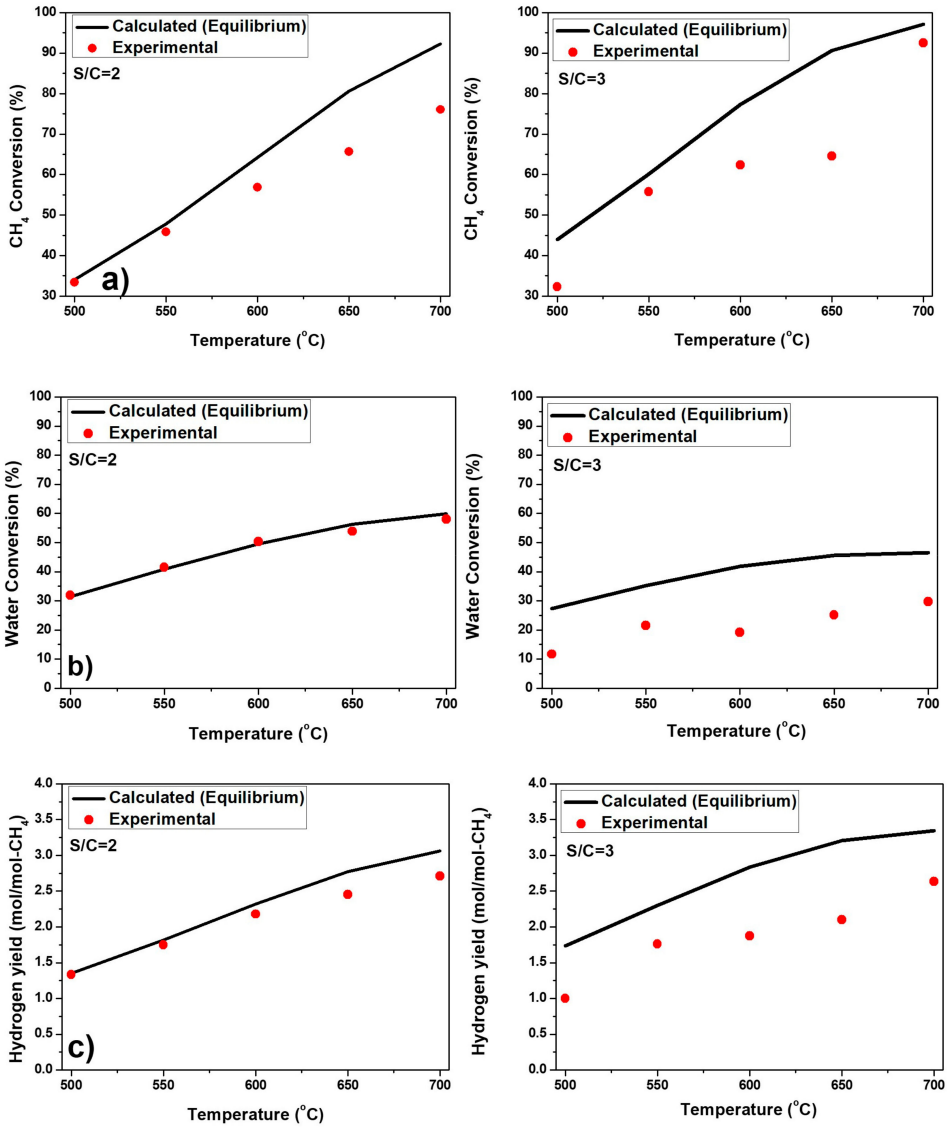

Figure 4. *Cont.*

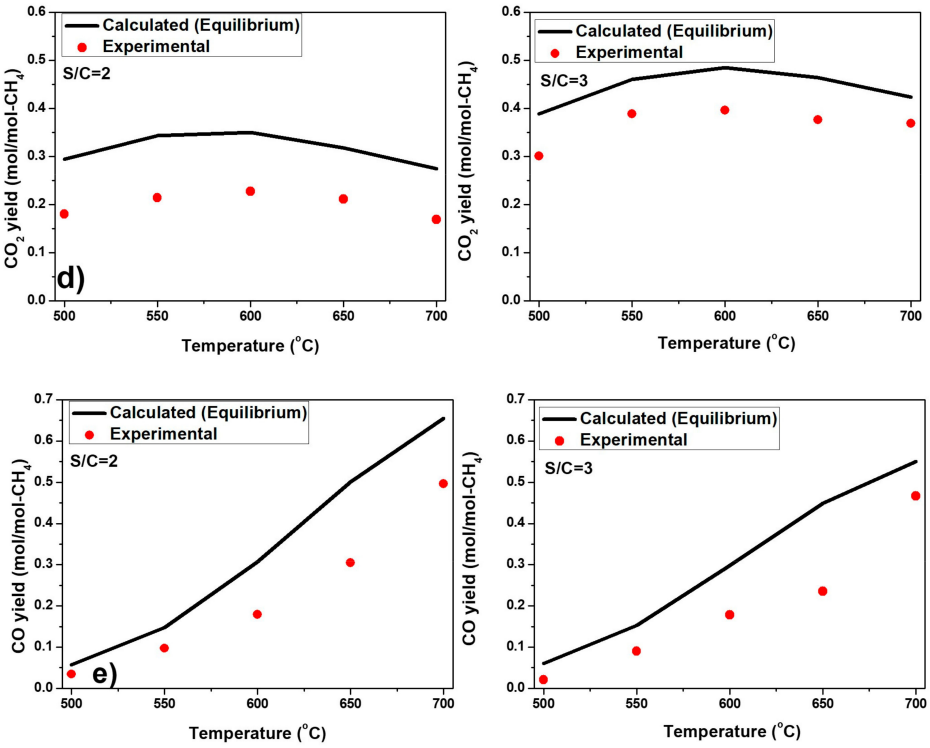

Figure 4. Experimental and calculated methane (equilibrium) steam reforming for 10%Ni/Al_2O_3 catalyst at various methane reaction temperatures for S/C of 2 and 3: (**a**) methane conversion, (**b**) water conversion, (**c**) hydrogen yield, (**d**) carbon dioxide yield and (**e**) carbon monoxide yield.

The above results showed that methane steam reforming and water gas shift are the main reactions producing CO_2, CO and hydrogen [5,6,51]. The temperature increase from 500 °C to 700 °C showed an increase in methane conversion and hydrogen production. The amount of CO_2 increased to maximum at 600 °C and then decreased, since the effects of water gas shift reaction are dropping at high temperature. Furthermore, CO is produced via the reverse water gas shift reaction and the methane steam reforming reactions [52]. The results showed a maximum hydrogen amount of 2.7 mol/mol-CH_4 at 700 °C and S/C = 2. The positive effect of increasing steam to carbon ratio was observed in the amount of CO_2 produced via water gas shift reaction since the increase in the amount of water would enhance CO_2 production [14,52]. Finally, the methane reaction showed high conversion at high temperature, corresponding to effective activation of C-H [53], and therefore, the reaction path appears to be independent of the H_2O partial pressure [7].

4.5. On-Off Catalytic Stability Test

In order to obtain the stability of the prepared catalysts, tests were performed for 20 h within three days (20 h in total) by switching the reaction furnace on and off in campaigns, running for several hours per day and shutting down the reaction furnace by leaving the catalyst under N_2 atmosphere overnight. The reason for using N_2 is to purge out the leftover gas from the reaction rig and ensure that the system will remain O_2 free. The selection of an elevated temperature for the On-Off tests is to study the temperature effects and operation time on the product yield and on the catalyst structure. Furthermore, to observe the performance of the catalyst after several shutdown operations. The reaction temperature was fixed at 700 °C and the ratio S/C was 2. Figure 5a shows that methane conversion was 87% during the first hour; then dropped to 75% in day one of operation. During the second day of operation, it was observed that the methane conversion has an increasing trend, that can be related to the reactivation of the catalyst during the reaction. Later, the conversion dropped down to 77%. It was also observed for day three that the reactivation occurred during the initial start-up

of the reaction then it stabilized. The dropping performance of the catalyst might be related to the carbon formation on the catalytic surface. The reactivation observed during the second and third day of operation, might be related to the remaining steam within the reactor during the switching off/on process and might also be related to the remaining H_2 during the cooling period.

Figure 5b shows the amount of hydrogen produced within 20 h during the On/Off tests. The maximum hydrogen yield was 2.88 mol/mol-CH_4 at the first hour of the stability test; then later, the hydrogen slightly decreased to an average value of 2.74 mol/mol-CH_4. Figure 5c,d show the produced amount of CO_2 and CO respectively. Both CO_2 and CO showed an opposite trend. The catalyst showed an increase in the produced CO_2 in the first 12 h then stabilized after a period of time of 1.5 h operation.

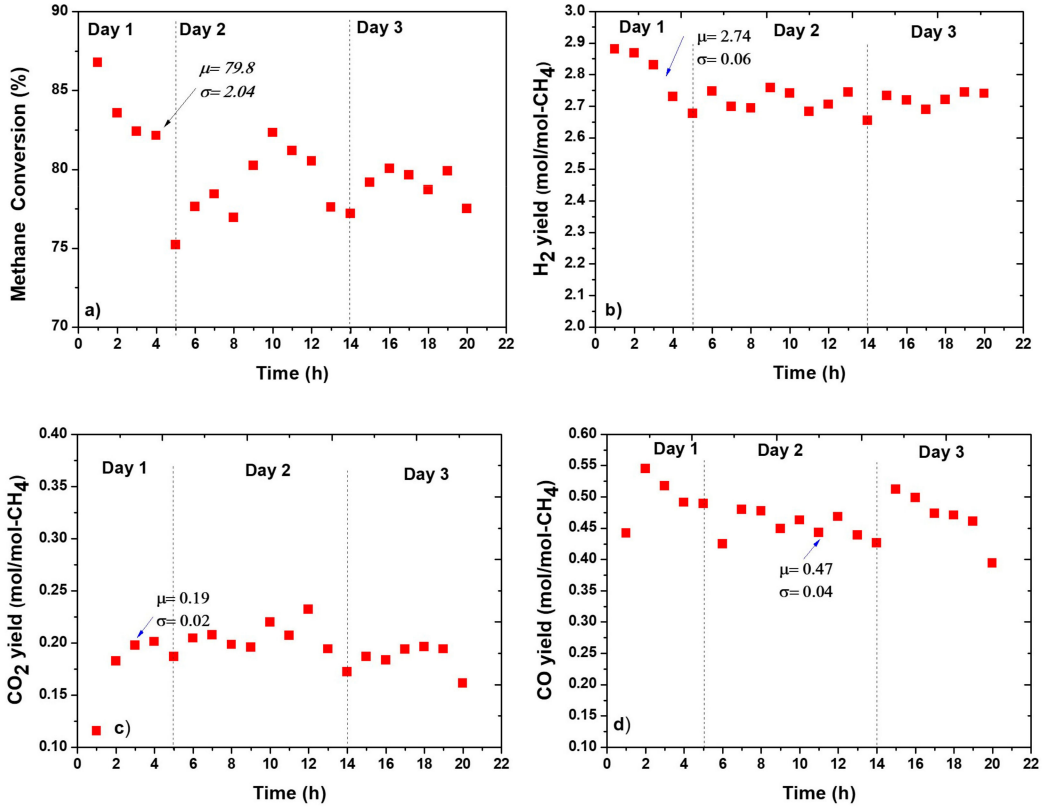

Figure 5. On-Off catalytic stability test of methane steam reforming at 700 °C and S/C of 2 for 10%Ni/Al_2O_3 catalyst, the values in the graph represent the average (μ) and variation (σ) for 20 h run: (**a**) Methane conversion (**b**) H_2 yield, (**c**) CO_2 yield, and (**d**) CO yield.

4.6. Carbon Formation

The carbon deposition on the catalytic surface could lead to reduction in the catalyst activity and the selectivity for the hydrogen produced during the reforming. Carbon is formed on the surface during the catalytic reaction, which leads to hydrocarbon species adsorption and dehydrogenation [54–57]. Table 2 presents the selectivity of carbon and the amount formed over the spent catalysts. The increase on the amount of steam in the reactants in the range of 2–5 was suggested, to reduce the amount of carbon formed on the catalytic surface for reaction temperatures above 800 °C [58]. The TGA results of the 10%Ni sample performed for long-term catalytic reactivity at 700 °C and S/C of 2 showed the carbon selectivity of 1.6%.

Table 2. Carbon selectivity on the used methane 10%Ni/Al_2O_3 catalyst reacted at 500–700 °C at S/C of 2 and 3.

	Carbon Selectivity				
	500 °C	**550 °C**	**600 °C**	**650 °C**	**700 °C**
S/C = 2	1.8%, 59.0 mg	2.0%, 63.0 mg	1.3%, 40.9 mg	1.8%, 57.3 mg	1.7%, 53.0 mg
S/C = 3	1.2%, 38.8 mg	0.7%, 21.7 mg	1.0%, 32.0 mg	0.7%, 21.7 mg	1.2%, 37.9 mg

The carbon formation depends on the particular catalyst and the operating conditions during the reaction. The carbon formation is increased with the number of carbon molecules in the reactants [55–57]. The carbon formation via methane steam reforming was categorized into three types; whisker, coke and gum carbon [54]. The main carbon formation routes are shown in Equations (28)–(30) [5] (methane decomposition (Equation (28)), Boudouard reaction (Equation (29)), CO reduction (Equation (30)).

The polymerization of CH_4 radicals would be possible at 500 °C at the beginning of the reaction resulting in active site blocking [59]. In contrast, the samples operated at 700 °C and S/C = 3 showed less carbon formation than the operated catalysts at S/C = 2 at the same temperature. It was observed in this case that the formation of carbon would be minimized by increasing the steam to carbon ratio at high reaction temperatures. Increasing the steam to carbon ratio can reduce the carbon formation, in agreement with the reported literature [58,60].

$$CH_4 \rightleftharpoons C + 2H_2, \qquad \Delta H^\circ_{298} = +75 \text{ kJ/mol} \tag{28}$$

$$2CO \rightleftharpoons C + CO_2, \qquad \Delta H^\circ_{298} = -172 \text{ kJ/mol} \tag{29}$$

$$CO + H_2 \rightleftharpoons C + H_2O, \qquad \Delta H^\circ_{298} = -131 \text{ kJ/mol} \tag{30}$$

It was suggested that an unstable carbide [13] intermediate can be formed on the supported nickel catalysts and remains attached to the metal and only the bulk carbide decomposes to form carbon [13,59]. The carbon formed via hydrocarbon decomposition (Equation (28)) was reported at temperatures above 600 °C [59]. In this case, a carbon atom diffuses rapidly through the carbide layer forming a constant carbon concentration within the metal particles. This can be inferred from the TGA results for catalysts operated for S/C of 2, at which the highest amount of carbon was formed.

5. Validation of the Numerical Model with the Experimental Results

The mathematical model suggested and described in the current work provides the temperature, pressure and species mass fraction profiles during the reaction. For the validation of the proposed mathematical model, simulation runs have been performed describing the steam reforming process at five different operation temperatures (500, 550, 600, 650 and 700 °C). A commercial finite element analysis software (COMSOL Multiphysics 5.0) used in order to incorporate the mathematical equations and to perform the simulation study. A stationary analysis was performed in a 2D-axisymmetric geometry. The dimensions of the geometry were selected to be exactly the same with the experimental dimensions described in Figure 1b. For the validation process, a S/C = 2 was introduced into the calculations. The molar fractions of the produced species H_2, CO and CO_2 were calculated and converted to H_2, CO and CO_2 yield (mol/mol_{CH4}) as described earlier. Figure 6a presents the comparison between the experimental results and the results obtained from the simulation study for the H_2 yield. According to the results, both the simulation and the experimental data follow the same trend and the maximum deviation between them does not exceed 8%. Figure 6c illustrates the comparison between the experimental results and the simulation data for the yield of the produced CO_2. As previously, the data present the same trend and the deviation is less than 6.4%. The same results are obtained for the yield of the produced CO (Figure 6b). Finally, Figures 6d and 6e present

the temperature and the pressure distribution of the produced H_2 respectively within the catalyst during the reforming reaction. For the temperature profile (Figure 6d) is visible that the temperature is lower in the core of the catalyst due to the endothermic nature of the reaction. The heat to maintain the reaction is provided externally from the furnace and this explains the fact that the temperature in Figure 6d is higher near the walls of the reactor where the heat transfer rate is higher.

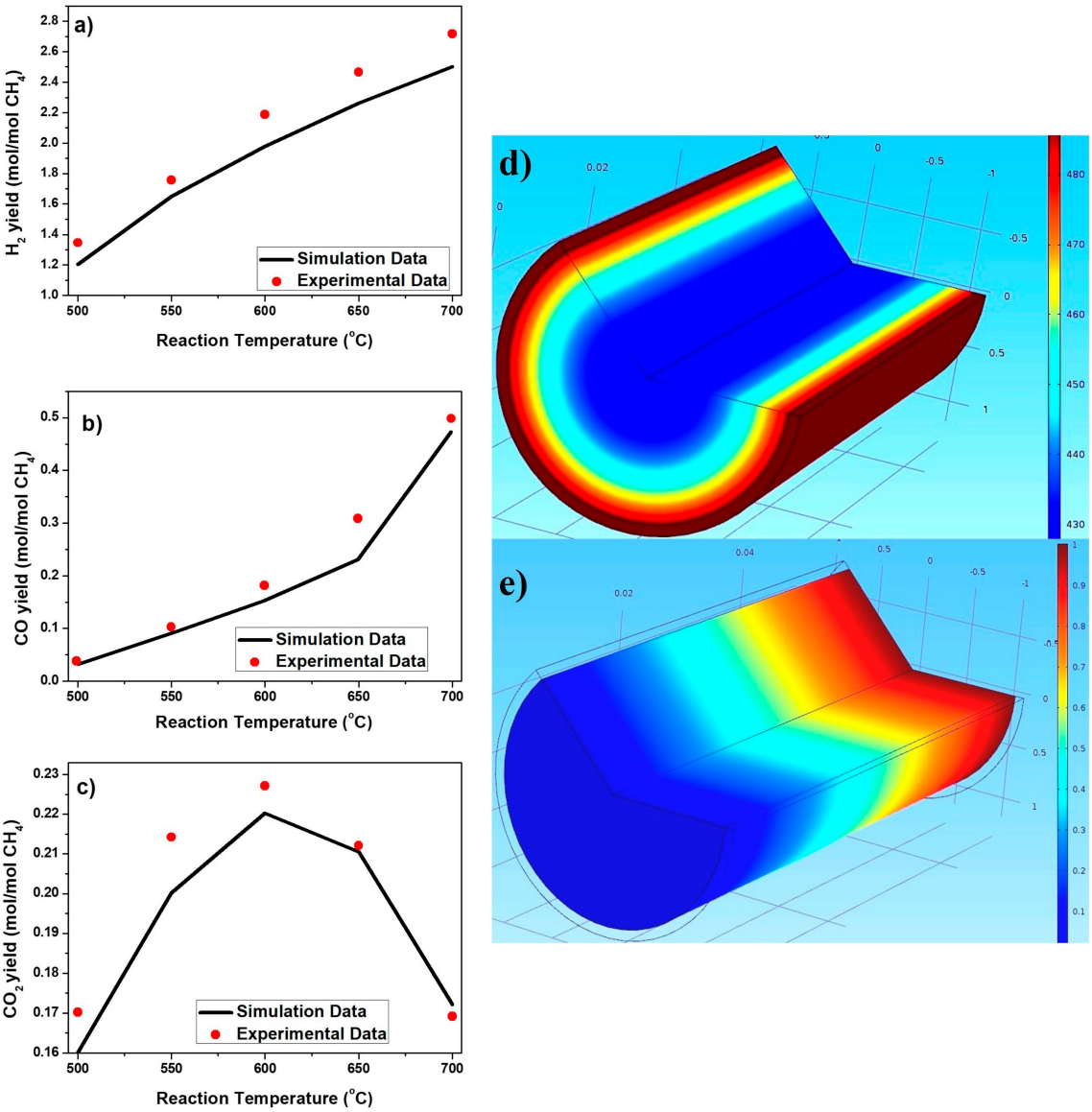

Figure 6. Validation of experimental results with the simulation data for 10%Ni/Al_2O_3 catalyst within 500–700 °C and S/C of 2 under atmospheric pressure; (**a**) H_2 yield, (**b**) CO yield, (**c**) CO_2 yield, (**d**) Catalyst bed temperature distribution and (**e**) H_2 pressure distribution.

6. Conclusions

The current work deals with the experimental and numerical study of low temperature methane steam reforming when using 10%Ni/Al_2O_3 catalyst. The numerical study used the equilibrium chemical analysis to evaluate the feasibility of the suggested reaction and a simulation study based on the kinetics and the thermodynamics of the reaction was performed to validate the results using commercial Finite Element Analysis (FEA) software (COMSOL Multiphysics). The low temperature methane steam reforming between 500 and 700 °C showed comprehensive results regarding methane

conversion and hydrogen yield production. Moreover, it was observed that low methane steam reforming was applicable for low Ni-loading catalysts with good stability and durability at low temperatures. The TGA results of the reacted catalysts at long stability test presented a carbon selectivity of 1.6%. Furthermore, the validation process of the experimental results and the data extracted from the simulation study showed very good agreement; proved that the mathematical model can efficiently describe the reforming reaction of the prepared catalyst.

Acknowledgments: The authors wish to express their gratitude to Joe Wood for his kind help and mentoring.

Author Contributions: Martin Khzouz has conducted the experiments and has done the INCA analysis. He also contributed on the writing of the manuscript; Evangelos I. Gkanas contributed to the development of the simulation study of the reaction and contributed on the writing of the manuscript.

Conflicts of Interest: The authors declare no conflict of interest.

Nomenclature

k	Rate Constant (s^{-1})
K	Adsorption Constant (s^{-1})
y	Mole Fraction
n	Mole Number
R	Kinetic Rate of Adsorption/Production (kg m^{-3}·s^{-1})
T	Temperature (K)
C_p	Specific Heat Capacity (J·kg^{-1}·K^{-1})
Q	Heat Source (W·m^{-3})
ΔH	Enthalpy of Formation/Deformation (J·mol^{-1})
ht	Heat Transfer Coefficient (W·m^{-2}·K^{-1})
M_m	Molar Mass (kg·mol^{-1})
P	Pressure (Pa)
u	Velocity (m·s^{-1})
E	Activation Energy (J·mol^{-1})
R_u	Gas Constant (J·mol^{-1}·K^{-1})
$\hat{n}$	Normal Vector
w	Concentration of Species (mol·m^{-3})
j	Mass Flux (kg·s^{-1}·m)
Subscripts	
i, j	Species
in	Inlet
out	Outlet
mix	Mixture
ext	External
bed	Bed (Reactor)
Greek Letters	
ρ	Density (kg·m^{-3})
μ	Dynamic Viscosity (Pa·s)
λ	Thermal Conductivity (W·m^{-1}·K^{-1})

References

1. Brown, L.F. A comparative study of fuels for on-board hydrogen production for fuel-cell-powered automobiles. *Int. J. Hydrogen Energy* **2001**, *26*, 381–397. [CrossRef]
2. Sjardin, M.; Damen, K.J.; Faaij, A.P.C. Techno-economic prospects of small-scale membrane reactors in a future hydrogen-fuelled transportation sector. *Energy* **2006**, *31*, 2523–2555. [CrossRef]
3. Ballard. Available online: http://www.ballard.com/ (accessed on 22 December 2017).
4. Rostrup-Nielsen, J. Reaction kinetics and scale-up of catalytic processes. *J. Mol. Catal. A: Chem.* **2000**, *163*, 157–162. [CrossRef]

5. Rostrup-Nielsen, J.R.; Sehested, J.; Nørskov, J.K. Hydrogen and synthesis gas by steam- and CO_2 reforming. In *Advances in Catalysis*; Academic Press: Cambridge, MA, USA, 2002; Volume 47, pp. 65–139.
6. Xu, J.; Froment, G.F. Methane steam reforming, methanation and water-gas shift: I. Intrinsic kinetics. *AIChE J.* **1989**, *35*, 88–96. [CrossRef]
7. Wei, J.; Iglesia, E. Isotopic and kinetic assessment of the mechanism of reactions of CH_4 with CO_2 or H_2O to form synthesis gas and carbon on nickel catalysts. *J. Catal.* **2004**, *224*, 370–383. [CrossRef]
8. Sehested, J. Four challenges for nickel steam-reforming catalysts. *Catal. Today* **2006**, *111*, 103–110. [CrossRef]
9. Rostrup-Nielsen, J.R. Production of synthesis gas. *Catal. Today* **1993**, *18*, 305–324. [CrossRef]
10. Ferreira-Aparicio, P.; Benito, M.J.; Sanz, J.L. New Trends in Reforming Technologies: From Hydrogen Industrial Plants to Multifuel Microreformers. *Catal. Rev.* **2005**, *47*, 491–588. [CrossRef]
11. Liu, X.; Yang, X.; Liu, C.; Chen, P.; Yue, X.; Zhang, S. Low-temperature catalytic steam reforming of toluene over activated carbon supported nickel catalysts. *J. Taiwan Inst. Chem. Eng.* **2016**, *65*, 233–241. [CrossRef]
12. Rostrup-Nielsen, J. 40 years in catalysis. *Catal. Today* **2006**, *111*, 4–11.
13. Trimm, D.L. Catalysts for the control of coking during steam reforming. *Catal. Today* **1999**, *49*, 3–10. [CrossRef]
14. Twigg, M.V. *Catalyst Handbook*, 2nd ed.; Wolfe Publishing Ltd.: London, UK, 1989.
15. Giannakeas, N.; Lea-Langton, A.; Dupont, V.; Twigg, M.V. Hydrogen from scrap tyre oil via steam reforming and chemical looping in a packed bed reactor. *Appl. Catal. B: Environ.* **2012**, *126*, 249–257. [CrossRef]
16. Daneshmand-Jahromi, S.; Rahimpour, M.; Meshksar, M.; Hafizi, A. Hydrogen Production from Cyclic Chemical Looping Steam Methane Reforming over Yttrium Promoted Ni/SBA-16 Oxygen Carrier. *Catalysts* **2017**, *7*, 286. [CrossRef]
17. S G Adiya, Z.I.; Dupont, V.; Mahmud, T. Chemical equilibrium analysis of hydrogen production from shale gas using sorption enhanced chemical looping steam reforming. *Fuel Process. Technol.* **2017**, *159*, 128–144. [CrossRef]
18. Hafizi, A.; Rahimpour, M.R.; Hassanajili, S. Hydrogen production via chemical looping steam methane reforming process: Effect of cerium and calcium promoters on the performance of Fe_2O_3/Al_2O_3 oxygen carrier. *Appl. Energy* **2016**, *165*, 685–694. [CrossRef]
19. Zieliński, J. Morphology of coprecipitated nickel/alumina catalysts with low alumina content. *Appl. Catal. A: Gen.* **1993**, *94*, 107–115. [CrossRef]
20. Lamber, R.; Schulzekloff, G. On the Microstructure of the Coprecipitated Ni-Al_2O_3 Catalysts. *J. Catal.* **1994**, *146*, 601–607. [CrossRef]
21. Znak, L.; Zieliński, J. The effect of potassium on Ni/Al_2O_3 catalyst in relation to CO/H_2 reaction. *Appl. Catal. A: Gen.* **2012**, *413–414*, 132–139. [CrossRef]
22. Borowiecki, T.; Denis, A.; Rawski, M.; Gołębiowski, A.; Stołecki, K.; Dmytrzyk, J.; Kotarba, A. Studies of potassium-promoted nickel catalysts for methane steam reforming: Effect of surface potassium location. *Appl. Surf. Sci.* **2014**, *300*, 191–200. [CrossRef]
23. Carrero, A.; Calles, J.A.; Vizcaíno, A.J. Hydrogen production by ethanol steam reforming over Cu-Ni/SBA-15 supported catalysts prepared by direct synthesis and impregnation. *Appl. Catal. A Gen.* **2007**, *327*, 82–94. [CrossRef]
24. Wu, P.; Li, X.; Ji, S.; Lang, B.; Habimana, F.; Li, C. Steam reforming of methane to hydrogen over Ni-based metal monolith catalysts. *Catal. Today* **2009**, *146*, 82–86. [CrossRef]
25. Zhang, M.; Ji, S.; Hu, L.; Yin, F.; Li, C.; Liu, H. Structural characterization of highly stable Ni/SBA-15 catalyst and its catalytic performance for methane reforming with CO_2. *Chin. J. Catal.* **2006**, *27*, 777–781. [CrossRef]
26. Yin, F.; Ji, S.; Wu, P.; Zhao, F.; Li, C. Deactivation behavior of Pd-based SBA-15 mesoporous silica catalysts for the catalytic combustion of methane. *J. Catal.* **2008**, *257*, 108–116. [CrossRef]
27. Sharma, P.O.; Abraham, M.A.; Chattopadhyay, S. Development of a novel metal monolith catalyst for natural gas steam reforming. *Ind. Eng. Chem. Res.* **2007**, *46*, 9053–9060. [CrossRef]
28. Liguras, D.K.; Kondarides, D.I.; Verykios, X.E. Production of hydrogen for fuel cells by steam reforming of ethanol over supported noble metal catalysts. *Appl. Catal. B: Environ.* **2003**, *43*, 345–354. [CrossRef]
29. Rostrupnielsen, J.R.; Hansen, J.H.B. CO_2-reforming of methane over transition metals. *J. Catal.* **1993**, *144*, 38–49. [CrossRef]
30. McMinn, T.E.; Moates, F.C.; Richardson, J.T. Catalytic steam reforming of chlorocarbons: Catalyst deactivation. *Appl. Catal. B: Environ.* **2001**, *31*, 93–105. [CrossRef]

31. Halabi, M.H.; De Croon, M.H.J.M.; Van Der Schaaf, J.; Cobden, P.D.; Schouten, J.C. Intrinsic kinetics of low temperature catalytic methane-steam reforming and water-gas shift over Rh/CeαZr1-αO_2 catalyst. *Appl. Catal. A: Gen.* **2010**, *389*, 80–91. [CrossRef]
32. Angeli, S.D.; Monteleone, G.; Giaconia, A.; Lemonidou, A.A. State-of-the-art catalysts for CH_4 steam reforming at low temperature. *Int. J. Hydrogen Energy* **2014**, *39*, 1979–1997. [CrossRef]
33. Nieva, M.A.; Villaverde, M.M.; Monzón, A.; Garetto, T.F.; Marchi, A.J. Steam-methane reforming at low temperature on nickel-based catalysts. *Chem. Eng. J.* **2014**, *235*, 158–166. [CrossRef]
34. Dal Santo, V.; Gallo, A.; Naldoni, A.; Guidotti, M.; Psaro, R. Bimetallic heterogeneous catalysts for hydrogen production. *Catal. Today* **2012**, *197*, 190–205. [CrossRef]
35. Andersson, M.; Paradis, H.; Yuan, J.; Sundén, B. Review of catalyst materials and catalytic steam reforming reactions in SOFC anodes. *Int. J. Energy Research* **2011**, *35*, 1340–1350. [CrossRef]
36. Li, D.; Nakagawa, Y.; Tomishige, K. Methane reforming to synthesis gas over Ni catalysts modified with noble metals. *Appl. Catal. A Gen.* **2011**, *408*, 1–24. [CrossRef]
37. Ma, Y.; Xu, Y.; Demura, M.; Hirano, T. Catalytic stability of Ni_3Al powder for methane steam reforming. *Appl. Catal. B Environ.* **2008**, *80*, 15–23. [CrossRef]
38. Guo, X.; Sun, Y.; Yu, Y.; Zhu, X.; Liu, C.J. Carbon formation and steam reforming of methane on silica supported nickel catalysts. *Catal. Commun.* **2012**, *19*, 61–65. [CrossRef]
39. Edwards, J.H.; Maitra, A.M. The chemistry of methane reforming with carbon dioxide and its current and potential applications. *Fuel Process. Technol.* **1995**, *42*, 269–289. [CrossRef]
40. Navarro, R.M.; Peña, M.A.; Fierro, J.L.G. Hydrogen production reactions from carbon feedstocks: Fossil fuels and biomass. *Chem. Rev.* **2007**, *107*, 3952–3991. [CrossRef] [PubMed]
41. Freni, S.; Calogero, G.; Cavallaro, S. Hydrogen production from methane through catalytic partial oxidation reactions. *J. Power Sources* **2000**, *87*, 28–38. [CrossRef]
42. Liu, C.J.; Ye, J.; Jiang, J.; Pan, Y. Progresses in the preparation of coke resistant Ni-based catalyst for steam and CO_2 reforming of methane. *ChemCatChem* **2011**, *3*, 529–541. [CrossRef]
43. Wu, H.; La Parola, V.; Pantaleo, G.; Puleo, F.; Venezia, A.; Liotta, L. Ni-Based Catalysts for Low Temperature Methane Steam Reforming: Recent Results on Ni-Au and Comparison with Other Bi-Metallic Systems. *Catalysts* **2013**, *3*, 563. [CrossRef]
44. Farshchi Tabrizi, F.; Mousavi, S.A.H.S.; Atashi, H. Thermodynamic analysis of steam reforming of methane with statistical approaches. *Energy Convers. Manag.* **2015**, *103*, 1065–1077. [CrossRef]
45. Yuan, Q.; Gu, R.; Ding, J.; Lu, J. Heat transfer and energy storage performance of steam methane reforming in a tubular reactor. *Appl. Thermal Eng.* **2017**, *125*, 633–643. [CrossRef]
46. Delgado, K.; Maier, L.; Tischer, S.; Zellner, A.; Stotz, H.; Deutschmann, O. Surface Reaction Kinetics of Steam- and CO_2-Reforming as Well as Oxidation of Methane over Nickel-Based Catalysts. *Catalysts* **2015**, *5*, 871–904. [CrossRef]
47. Brunauer, S.; Emmett, P.H.; Teller, E. Adsorption of gases in multimolecular layers. *J. Am. Chem. Soc.* **1938**, *60*, 309–319. [CrossRef]
48. Yuan, J.; Lv, X.; Yue, D.; Sunden, B. Transport phenomena coupled by chemical reactions in methane reforming ducts. *Trans. Phenomena* **2009**, *11*, 39–50.
49. Roh, H.-S.; Jun, K.-W.; Dong, W.-S.; Chang, J.-S.; Park, S.-E.; Joe, Y.-I. Highly active and stable Ni/Ce–ZrO_2 catalyst for H_2 production from methane. *J. Mol. Catal. A: Chem.* **2002**, *181*, 137–142. [CrossRef]
50. Ye, J.; Li, Z.; Duan, H.; Liu, Y. Lanthanum modified Ni/γ-Al_2O_3 catalysts for partial oxidation of methane. *J. Rare Earths* **2006**, *24*, 302–308. [CrossRef]
51. Yablonskii, G.S.V.; Bykov, V.I.; Elokhin, V.I.; Gorban, A.N. *Kinetic Models of Catalytic Reactions*; Elsevier: Amsterdam, The Netherlands, 1991; Volume 32.
52. Matsumura, Y.; Nakamori, T. Steam reforming of methane over nickel catalysts at low reaction temperature. *Appl. Catal. A Gen.* **2004**, *258*, 107–114. [CrossRef]
53. Wei, J.; Iglesia, E. Structural requirements and reaction pathways in methane activation and chemical conversion catalyzed by rhodium. *J. Catal.* **2004**, *225*, 116–127. [CrossRef]
54. Rostrup-Nielsen, J.R. Sulfur-passivated nickel catalysts for carbon-free steam reforming of methane. *J. Catal.* **1984**, *85*, 31–43. [CrossRef]

55. Bengaard, H.S.; Nørskov, J.K.; Sehested, J.; Clausen, B.S.; Nielsen, L.P.; Molenbroek, A.M.; Rostrup-Nielsen, J.R. Steam reforming and graphite formation on Ni catalysts. *J. Catal.* **2002**, *209*, 365–384. [CrossRef]
56. Sidjabat, O.; Trimm, D.L. Nickel–magnesia catalysts for the steam reforming of light hydrocarbons. *Top. Catal.* **2000**, *11–12*, 279–282. [CrossRef]
57. Trimm, D.L. The formation and removal of coke from nickel catalyst. *Catal. Rev.* **1977**, *16*, 155–189. [CrossRef]
58. Trimm, D.L. Coke formation and minimisation during steam reforming reactions. *Catal. Today* **1997**, *37*, 233–238. [CrossRef]
59. Bartholomew, C.H. Carbon deposition in steam reforming and methanation. *Catal. Rev.* **1982**, *24*, 67–112. [CrossRef]
60. Sasaki, K.; Teraoka, Y. Equilibria in Fuel Cell Gases: I. Equilibrium Compositions and Reforming Conditions. *J. Electrochem. Soc.* **2003**, *150*, A878–A884. [CrossRef]